IEEE Access
Multidisciplinary | Rapid Review | Open Access Journal

Received November 21, 2019, accepted December 23, 2019, date of publication December 31, 2019,
date of current version January 17, 2020.

Digital Object Identifier 10.1109/ACCESS.2019.2963369

High-Resolution Hyperspectral Microscopic Imaging With Single Acousto-Optic Tunable Filter Based on Double Filtering

XIAOFA ZHANG[1], CHUNGUANG ZHANG[1], YUPUYUN WANG[1], HAO WANG[1,2], ZHENFEI SHENG[1], ZHIWEI TAN[1], WEIJIE QIU[1], XI HUANG[1], PENGCHONG WANG[1,2], WENYAO LIU[3], HAIPING TONG[1], YUHAO LIU[1], AND XIANSHENG WANG[1]

[1]Key Laboratory of Optoelectronic Science and Technology for Medicine, Fujian Provincial Key Laboratory of Photonics Technology, Fujian Provincial Engineering Technology Research Center of Photoelectric Sensing Application, College of Photonic and Electronic Engineering, Ministry of Education, Fujian Normal University, Fujian 350007, China
[2]CAS Key Laboratory of Spectral Imaging Technology, Chinese Academy of Sciences, Xi'an 710119, China
[3]Fujian Normal University Hospital, Fuzhou 350007, China

Corresponding authors: Chunguang Zhang (cgzhang@fjnu.edu.cn) and Hao Wang (haowang@fjnu.edu.cn)

This work was supported in part by the Special Funds of the Central Government Guiding Local Science and Technology Development under Grant 2017L3009, in part the Natural Science Foundation of Fujian Province, China, under 2017J01745, in part by the Program for Changjiang Scholars and Innovative Research Team in University (IRT_15R10), in part the Open Research Fund of Fujian Provincial Engineering Technology Research Center of Photoelectric Sensing Application under Grant 2018002 and Grant 2018004, in part by the Open Research Fund of CAS Key Laboratory of Spectral Imaging Technology under Grant LSIT201809D, in part by the Open Research Fund of Key Laboratory of Optoelectronic Science and Technology for Medicine of Ministry of Education under Grant JYG1803, and in part by the College Students Innovation Training Program of Fujian Normal University under Grant cxxl-2019153.

ABSTRACT Hyperspectral imaging is a technique that integrates multiple spectral bands and image information. Its applications range from improving the accuracy of cancer diagnosis to testing the quality of products. Here, we introduce a double-filtering technique that provides high-resolution diagnostic histological images within minutes. The hyperspectral microscopic imaging system is built based on an acousto-optic tunable filter (AOTF). The optimized system is analyzed from the perspective of spectrum and imaging. The spectral resolution can be improved by 37.08 % to 59.95% in the visible light range. The side lobe is obviously inhibited and the purity of spectrum is improved. Furthermore, the example of hyperspectral microscopic imaging is demonstrated with unstained gastric cancer tissue sections to assess the ability of the system in terms of its spectral performances and image quality. The microscopic imaging results of single filtering optical path system and single crystal double filtering optical path system are compared. In general, the optimized double filtering system achieves excellent performance in bandwidth compression and side lobe suppression, especially the first application of hyperspectral microscopy combined with microscope in the visible light range.

INDEX TERMS Acousto-optical device, birefringence, high-resolution imaging, optical device fabrication.

I. INTRODUCTION

Hyperspectral imaging (HSI) technology is a growing field integrating multiple spectral bands and spatial information. Its applications include remote sensing, agriculture, resource exploration, environmental monitoring, cancer detection, etc [1]–[6].

At present, acousto-optic tunable filter (AOTF) is more and more widely used in hyperspectral imaging field [7]–[10]. It is attributed to advantages of AOTF device with large angular aperture, no moving parts, high diffraction efficiency, and rapid frequency tuning characteristics in wide spectral range [11]–[14].

Spectral bandwidth, side lobe and diffraction efficiency are the main parameters used to assess the capability of AOTF. In order to achieve high resolution and hyperspectral images, the high resolution hyperspectral microscopic imaging system with single crystal based on double filtering technology is designed and optimized. In the previous research, the theory and partial experimental verification of double filtering have

The associate editor coordinating the review of this manuscript and approving it for publication was Jenny Mahoney.

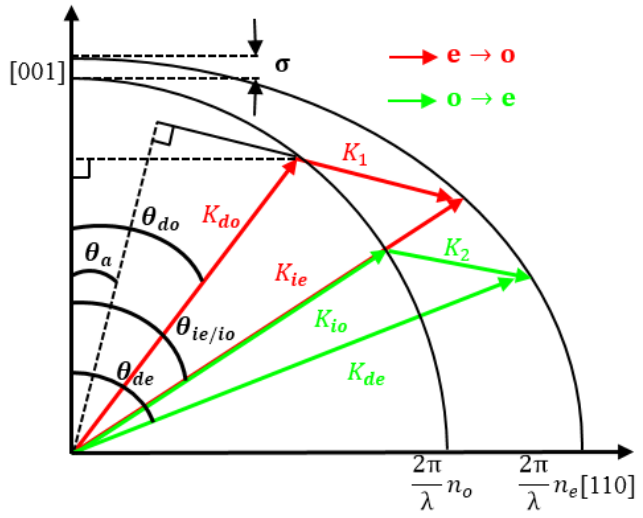

FIGURE 1. Wave vector diagram of single and double filtering of AOTF.

been realized. The double filtering technology in this paper includes filtering technology based on two AOTFs and a single AOTF. For the former, C. Zhang et al introduced the double filtering with two AOTFs in tandem in 2008 [15]. Recently, an imaging system for measuring two-dimensional surface temperature distribution of microscopic samples is introduced [16]. Wang implemented a hyperspectral imaging for the far field imaging with two AOTFs [17], [18]. In related fields, A. Jullien introduced a polarized hyperspectral imaging with two cascaded liquid crystal cells [19]. For the latter, You described the double filtering based on AOTF and confirmed the feasibility of the method with a He-Ne laser and a diode laser [20]. C. Justine determined the radio frequency driving for optimum diffraction efficiency for different wavelengths [21]. In 2018, an imaging system with resolution target was established based on single AOTF and showed a double filtering image at 484.0 nm without the use of microscope [22]. However, hyperspectral microscopic imaging system with high resolution and high quality images based on a single AOTF has not been reported.

Non-collinear AOTF is based on uniaxial birefringent crystal. The acousto-optic (AO) crystal material used in our device is tellurium dioxide (TeO2), which is an outstanding AO crystal material and is completely transparent in the range of visible light [23]–[26].The wavelength range of self-designed AOTF is 400-1000 nm and is controlled by loaded radio frequency (RF) signal. The RF scanning range is 65 MHz - 220 MHz.

The wave vector diagram and vector relationship of single and double filtering of AOTF are shown in Fig. 1. K_{do},K_{ie} and K_1 are the diffracted wave vector, the incident optical wave vector and acoustic wave vector of the first AO interaction (e → o), respectively. Extraordinary light is the incident light for the first AO interaction. K_{io}, K_{de} and K_2 are the incident optical wave vector, the diffracted wave vector and acoustic wave vector of the second AO interaction (o → e), respectively. The diffracted light obtained by first AO interaction acts as the incident light of the second AO interaction. $\theta_{do/de}$ and $\theta_{ie/io}$ represent the diffracted and the incident polar angles, respectively. $\theta_a(\theta_a = 9.7°)$ is the angle between the K_1 and the [110]. The physical constant σ is related to the rotation ability of the AO crystal.

In this paper, on the basis of the previous work [27], we have successfully realized the micro-imaging in the broadband light range by combining the double filtering system with the inverted microscope for the first time. We present an optimized hyperspectral microscopic imaging system with single AOTF based on double filtering for increased spectral resolution, decreased side lobe and improved image quality [9]. Examples of hyperspectral microscopic imaging are demonstrated with unstained gastric cancer tissue sections for the first time by using single crystal double filter technology. The microscopic imaging results of single filtering optical path system and single crystal double filtering optical path system are compared.The proposed single crystal double filtering system has many advantages, such as low cost, high resolution, high quality image, and compact, integrated with microscope.

II. EXPERMEBTAL SETUP

The hyperspectral microscopic imaging system with single AO device based on double filtering technology is shown in Fig. 2. The illustration shows a detailed system configuration of the optimized single acousto-optic crystal double filtering with an inverted microscope (Nikon, TE2000-U). The principle and process of the whole experiment can be summarized as follows. A wide band light source generated by the halogen lamp (60W) mounted on a microscope is used in our experiment, with spectra from 400 - 1000 nm. The white light enters our optimized optical system after passing through the sample, objective lens and mirror1. After being collimated by the collimation system, white light passes through polarizer 1 and becomes linearly polarized light with horizontal polarization. Horizontally polarized light (extraordinary light, e light) enters the AOTF and the first AO interaction occurs with ultrasonic wave controlled by radio frequency (RF) signal generator. A diffracted beam and a zero-order transmitted beam will be obtained by the first AO interaction (e → o). According to the momentum matching condition, the diffraction beam of narrow band (ordinary light, o light) is produced.

The optical loop is composed of two silver mirrors and two polarizing beam splitters (PBS) in Fig. 2, and the diffracted light (ordinary light, o light) produced by the first AO interaction enters the AOTF as the incident light of the second AO interaction. Lens 2 and lens 3 will collimate the diffracted light, ensuring that the incident light entering the device for the second acousto-optic interaction is collimated beam. The o light enters the device to conduct the second AO interaction (o → e). In this way, a narrower diffracted light is produced and the polarization states of incident and diffracted light are perpendicular. Finally, the e light is received by a colour CCD (Nikon, DS-5M, 3.4 μm/ pixel) after passing through

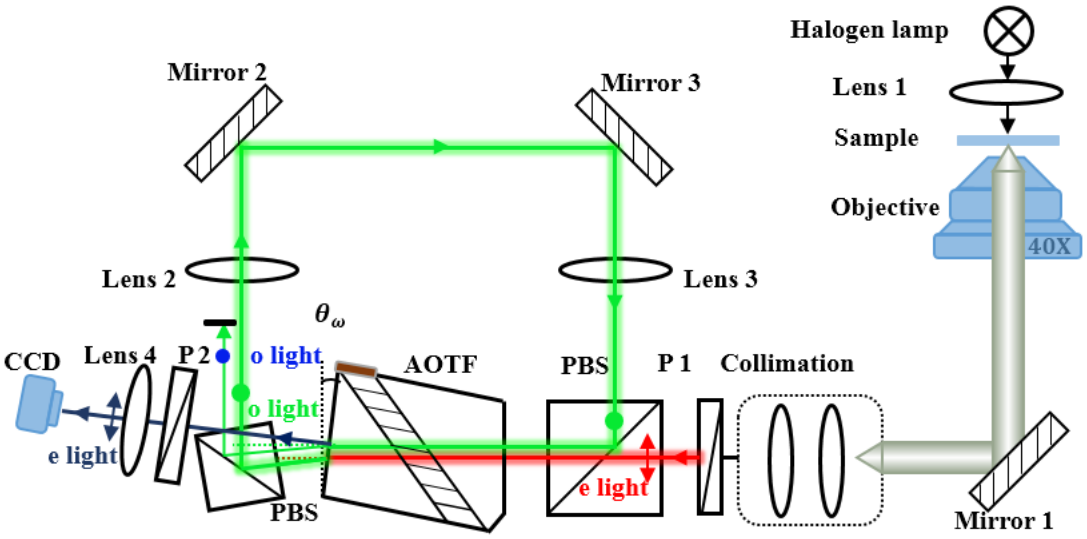

FIGURE 2. Hyperspectral microscopic imaging double filtering system with an AOTF.

polarizer 2 and lens 4.The technology based on an AOTF is named single crystal double filtering. Green o light and blue o light represent the diffracted light obtained by the first AO interaction and the transmitted light of the second AO interaction, respectively. In Fig. 2, the black baffle is used to block unwanted light, which is convenient for subsequent research. θ_ω ($\theta_\omega = 6.323°$) is an optical wedge angle, which is designed to reduce the drift of the diffracted light.

The refractive index of incident and diffracted light can be expressed as [17]:

$$n_{ie} = \left[\frac{\cos^2\theta_{ie}}{n_o^2(1+\sigma)^2} + \frac{\sin^2\theta_{ie}}{n_e^2}\right]^{-\frac{1}{2}} \tag{1}$$

$$n_{do} = \left[\frac{\cos^2\theta_{io}}{n_o^2(1-\sigma)^2} + \frac{\sin^2\theta_{do}}{n_o^2}\right]^{-\frac{1}{2}} \tag{2}$$

where n_{ie} represents the refractive index of extraordinary incident light. The n_{do} represents the refractive index of the diffracted light of extraordinary incident light. The n_e and n_o are the extraordinary and ordinary refractive indices of TeO2 crystal, respectively. They are described as:

$$n_e = \left[1 + \frac{2.82338\lambda^2}{\lambda_o^2 - 0.1342^2} + \frac{1.5402\lambda^2}{\lambda_o^2 - 0.2638^2}\right]^{\frac{1}{2}} \tag{3}$$

$$n_o = \left[1 + \frac{2.5848\lambda^2}{\lambda^2 - 0.1342^2} + \frac{1.1568\lambda^2}{\lambda^2 - 0.2638^2}\right]^{\frac{1}{2}} \tag{4}$$

In our experiment, the spectral bandwidth of AO device can be written as [28]:

$$\Delta\lambda = \frac{1.8\pi\lambda^2}{DLsin^2\theta_i} \tag{5}$$

where the dispersion term $\lambda\lambda D = 2\pi[\Delta n - (\partial(\Delta n)/\partial)]$,and $\Delta n = n_e - n_o$. L and θ_i are the AO interaction length and the incident angle, respectively.

$$R = \frac{\lambda}{\Delta\lambda} \tag{6}$$

Equation (6) is the formula for spectral resolution. Where λ is the wavelength of the diffracted light and $\Delta\lambda$ represents the spectral bandwidth.

III. RESULTS

In the following section we report on the performances of the single and double filtering with a TeO2 crystal, including the tuning relationship of the wavelength with RF, spectral bandwidth, spectral resolution and side lobe, using broadband light source. On one hand, we show the compression of spectral bandwidth and the suppression of side-lobe of double filtering technology. On the other hand, examples of hyperspectral microscopic imaging is demonstrated to illustrate the improvement of resolution and image quality based on an AOTF double filtering.

A. SPECTRAL ACQUISITION AND ANALYSIS

We carry out experiments according to the hyperspectral microscopic imaging double filtering system with an AOTF shown in Fig. 2. The first AO interaction path is shown in red line. The unpolarized light passes through P1 and PBS successively. The e light is selected as the incident light of the first AO interaction, and the diffracted light produced is o light. P1 and P2 are Polaroids. The output beam is received by a spectrometer (HR4000, Ocean Optics). The measurement interval of experimental data points is 1MHz. The RF range set in our experiment is 92 - 180 MHz. The wavelength range is 756.66 - 450.55 nm. Figure 3 is the tuning relationship of the wavelength with RF of single and double filtering. The e light and o light are the incident light of single and double filtering, respectively.

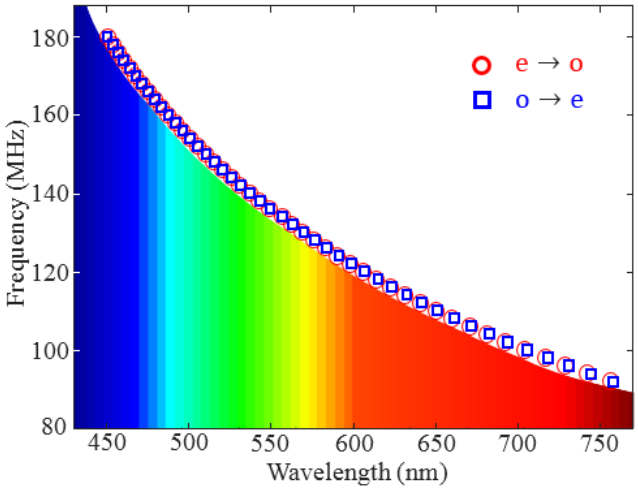

FIGURE 3. Tuning relationship between single and double filtering wavelength and RF.

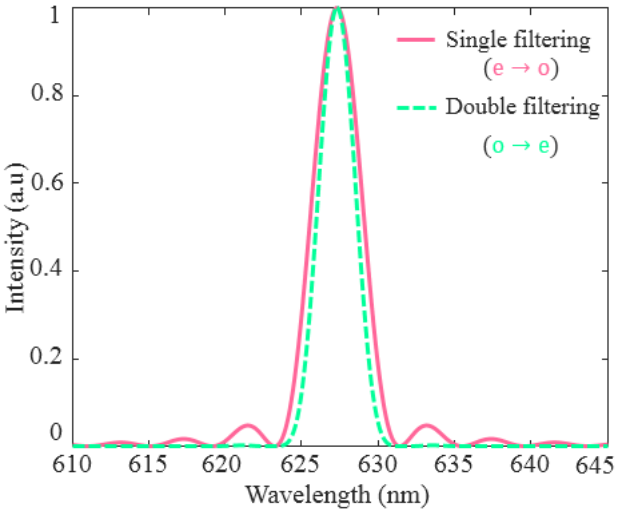

FIGURE 4. Single and double filtering theoretical spectra at the central wavelength of 627.33 nm.

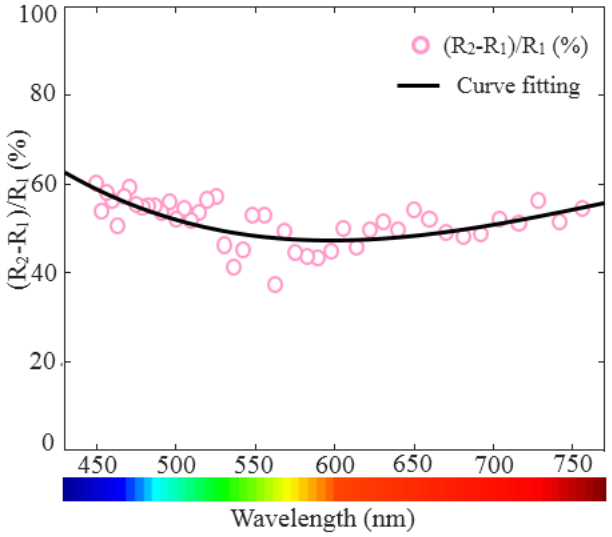

FIGURE 5. The percentage of spectral resolution improvement of double filtering over single filtering in the visible region.

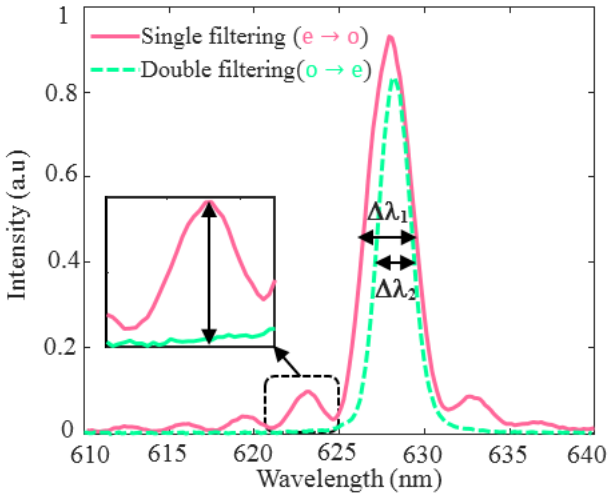

FIGURE 6. Single and double filtering experimental measurement spectra with wavelength of 627.33 nm and 628.38 nm (RF = 115MHz).

Figure 4 is the single and double filtering theoretical spectra with the wavelength of 627.33 nm. The solid and dashed lines represent the theoretical spectra of single and double filtering, respectively. The spectrum of single filtering, which has the typical sinc^2 shape with a distinct side lobe on both sides of the main peak. As in Fig 5, the central wavelengths of the spectrum measured by the single and double filtering are 627.33 nm and 628.38 nm. RF is 115 MHz. The solid line and the dashed line are the experimental measured results of the single double filtering. The solid line represents the result of the first AO interaction (e → o). The dashed line represents the result of the diffracted light (o light) produced by the first AO interaction as the incident light of the second AO interaction (o → e). From the experimental results in Fig. 5, it can be concluded that the spectral bandwidth is significantly narrowed from 2.96 nm to 1.99 nm and the side lobes are significantly suppressed by 11.9 dB from −10.34 dB to −22.24 dB. $\Delta\lambda 1$ and $\Delta\lambda 2$ represent spectral bandwidth of the single and double filtering, respectively. The spectral resolution increases with the decrease of spectral bandwidth. The spectral bandwidth described above represents the full width at half maximum.

We compare the spectral resolution of single and double filtering based on the above experimental data. Compared with single filtering, the spectral resolution of single crystal double filtering is increased by 37.08 % to 59.95 %, shown in Fig. 6.

B. HYPERSPECTRAL IMAGING

In our experiment, the sample is a paraffin slide with the thickness of 5um. Hyperspectral microscopic imaging of

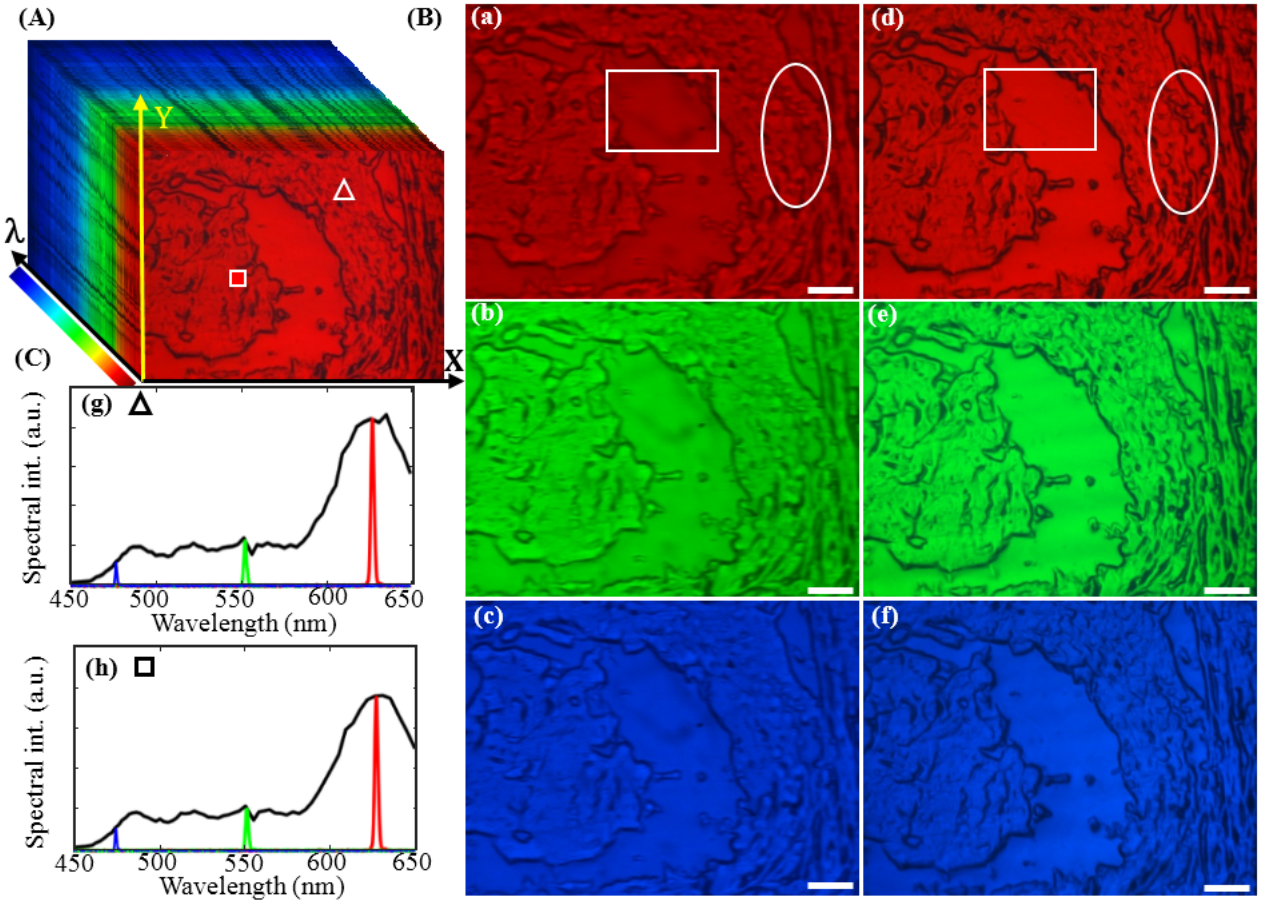

FIGURE 7. Hyperspectral microscopic imaging of non-staining gastric cancer. (A) The hyperspectral data cube of double filtering. (B) The hyperspectral microscopic images of single filtering (a, b, c) and double filtering (d, e, f). (C) Transmission spectra of sample. Scale bar = 25 um.

tissue section of unstained gastric cancer is performed with single and double filtering, respectively. In each case, when images are collected, the RF of AOTF is scanned from 110 MHz to 180 MHz with an interval of 1MHz, and the RF driving voltage is maintained at 2.5 V. The wavelength range is 650 - 450.55 nm. Figure 7 is the results of hyperspectral microscopic imaging of non-staining gastric cancer. The three-dimensional hyperspectral data cube (n = 71) is shown in Fig. 7 (A). Figure 7 (B) shows the results of hyperspectral images. (a),(b) and (c) are the results of single filtering hyperspectral imaging with RF of 115MHz, 135 MHz, and 165 MHz respectively, corresponding wavelengths are 627.33 nm, 552.15 nm and 477.42 nm, respectively. The results of single crystal double filtering hyperspectral microscopic imaging are (d), (e) and (f) with RF of 115 MHz, 135 MHz, and 165 MHz respectively, corresponding wavelengths are 628.38 nm, 553.21 nm and 477.57 nm respectively. Figure 7 (C) is the transmission spectra of sample. (g) and (h) are respectively the transmission spectra of the two regions of interest (ROI) in Fig. 7 (A). For example, the triangle icon in (g) corresponds to the triangle ROI in A. The colors of the three spectra lines in (g) and (h) correspond to the ROI of (d), (e) and (f) in Fig. 7 (B), respectively.

Compared with the results of single filtering hyperspectral imaging, we can also notice that the single crystal double filtering technology shows more detailed information, for example, the texture and edges of the tissue are clearer, and has significant improvement in resolution, image quality and contrast enhancement. The spread of the diffracted angle is reduced by increasing the spectral purity, that is, by compressing the spectral bandwidth. Therefore, the image resolution will be improved. The higher the spectral resolution is, the better the imaging resolution is. When RF is maintained at 115 MHz, 135 MHz and 165 MHz, the image resolution of double filtering is improved by 51.1%, 52.87% and 55.16%, respectively [29].

IV. CONCLUSION

In conclusion, we have optimized hyperspectral microscopic imaging system with an AO device based on double filtering and experimentally demonstrated the results of single and double filtering with single AOTF. From the perspective of spectrum, the compression of spectral bandwidth and the suppression of side lobe by single crystal double filtering technique are analysed. Meanwhile, this is the first time to successfully achieve hyperspectral microscopic images of

unstained gastric cancer tissue samples in the visible region based on double filtering technique. The single crystal double filtering technology has obvious advantages in resolution and imaging quality.

Prospectively, with the development optimization of integration technology, we anticipate that hyperspectral microscopic imaging technology based on single AO crystal double filtering has the capacity to provide additional information on the accuracy of medical diagnosis and can promote further applied research in this field.

REFERENCES

[1] G. D. Boreman, "Classification of imaging spectrometers for remote sensing applications," *Opt. Eng.*, vol. 44, no. 1, Jan. 2005, Art. no. 013602.

[2] A. Gowen, C. Odonnell, P. Cullen, G. Downey, and J. Frias, "Hyperspectral imaging—An emerging process analytical tool for food quality and safety control," *Trends Food Sci. Technol.*, vol. 18, no. 12, pp. 590–598, Dec. 2007.

[3] G. A. Blackburn, "Hyperspectral remote sensing of plant pigments," *J. Experim. Botany*, vol. 58, no. 4, pp. 855–867, Sep. 2006.

[4] M. Huang, C. He, Q. Zhu, and J. Qin, "Maize seed variety classification using the integration of spectral and image features combined with feature transformation based on hyperspectral imaging," *Appl. Sci.*, vol. 6, no. 6, p. 183, Jun. 2016.

[5] M. E. Martin, M. B. Wabuyele, and K. Chen, "Development of an advanced hyperspectral imaging (HIS) system with applications for cancer detection," *Ann. Biomed. Eng.*, vol. 34, no. 6, pp. 1061–1068, Jun. 2006.

[6] G. Lu, L. Halig, D. Wang, X. Qin, Z. G. Chen, and B. Fei, "Spectral-spatial classification for noninvasive cancer detection using hyperspectral imaging," *J. Biomed. Opt.*, vol. 19, no. 10, Oct. 2014, Art. no. 106004.

[7] N. Gupta and V. Voloshinov, "Hyperspectral imaging performance of a TeO_2 acousto-optic tunable filter in the ultraviolet region," *Opt. Lett.*, vol. 30, no. 9, p. 985, May 2005.

[8] N. Gupta and V. Voloshinov, "Hyperspectral imager, from ultraviolet to visible, with a KDP acousto-optic tunable filter," *Appl. Opt.*, vol. 43, no. 13, p. 2752, May 2004.

[9] C. Zhang, H. Wang, J. Huang, and Q. Gao, "The visible to the near infrared narrow band acousto-optic tunable filter and the hyperspectral microscopic imaging on biomedicine study," *J. Opt.*, vol. 16, no. 12, Dec. 2014, Art. no. 125303.

[10] R. Abdlaty, L. Doerwald-Munoz, A. Madooei, S. Sahli, S.-C.-A. Yeh, J. Zerubia, R. K. W. Wong, J. E. Hayward, T. J. Farrell, and Q. Fang, "Hyperspectral imaging and classification for grading skin erythema," *Frontiers Phys.*, vol. 6, no. 72, pp. 1–10, Aug. 2018.

[11] I. C. Chang, "Noncollinear acousto-optic filter with large angular aperture," *Appl. Phys. Lett.*, vol. 25, no. 7, pp. 370–372, Oct. 1974.

[12] I. C. Chang, "Analysis of the noncollinear acousto-optic filters," *Electron. Lett.*, vol. 11, no. 5, pp. 617–618, Dec. 1975.

[13] C. Zhang, Z. Zhang, H. Wang, and Y. Yang, "Analysis of the optimum optical incident angle for an imaging acousto-optic tunable filter," *Opt. Express*, vol. 15, no. 19, 2007, Art. no. 11883.

[14] N. Gupta and D. R. Suhre, "Notch filtering using a multiple passband AOTF in the SWIR region," *Appl. Opt.*, vol. 55, no. 28, p. 7855, Oct. 2016.

[15] C. Zhang, Z. Zhang, H. Wang, and Y. Yang, "Development of double-filtering imaging acousto-optic tunable filter with increased spectral resolution," *Opt. Lett.*, vol. 33, no. 18, p. 2020, Sep. 2008.

[16] A. S. Machikhin, P. V. Zinin, A. V. Shurygin, and D. D. Khokhlov, "Imaging system based on a tandem acousto-optical tunable filter for *in situ* measurements of the high temperature distribution," *Opt. Lett.*, vol. 41, no. 5, p. 901, Mar. 2016.

[17] P. Wang and Z. Zhang, "Double-filtering method based on two acousto-optic tunable filters for hyperspectral imaging application," *Opt. Express*, vol. 24, no. 9, p. 9888, May 2016.

[18] P. Wang and Z. Zhang, "Hyperspectral imaging performance based on two TeO_2 acousto-optic tunable filters," *Appl. Opt.*, vol. 56, no. 6, p. 1647, Feb. 2017.

[19] A. Jullien, R. Pascal, U. Bortolozzo, N. Forget, and S. Residori, "High-resolution hyperspectral imaging with cascaded liquid crystal cells," *Optica*, vol. 4, no. 4, p. 400, Apr. 2017.

[20] J.-W. You, J. Ahn, S. Kim, and D. Kim, "Efficient double-filtering with a single acousto-optic tunable filter," *Opt. Express*, vol. 16, no. 26, Dec. 2008, Art. no. 21505.

[21] J. Champagne, J.-C. Kastelik, S. Dupont, and J. Gazalet, "Study of the spectral bandwidth of a double-pass acousto-optic system [invited]," *Appl. Opt.*, vol. 57, no. 10, p. C49, Apr. 2018.

[22] C. Zhang, H. Wang, Z. Zhang, J. Yuan, L. Shi, Z. Sheng, and X. Zhang, "Narrowband double-filtering hyperspectral imaging based on a single AOTF," *Opt. Lett.*, vol. 43, no. 9, p. 2126, May 2018.

[23] V. B. Voloshinov, K. B. Yushkov, and B. B. J. Linde, "Improvement in performance of a TeO2 acousto-optic imaging spectrometer," *J. Opt. A, Pure Appl. Opt.*, vol. 9, no. 4, pp. 341–347, Mar. 2007.

[24] T. Yano and A. Watanabe, "Acousto-optic TeO_2 tunable filter using far off axis anisotropic Bragg diffraction," *Appl. Opt.*, vol. 15, no. 9, pp. 2250–2258, Sep. 1976.

[25] N. Uchida, "Optical properties of single–crystal paratellurite (TeO_2)," *Phys. Rev. B, Condens. Matter*, vol. 4, no. 10, pp. 3736–3745, Jul. 2002.

[26] C. Zhang, Z. Zhang, Y. Yang, and H. Wang, "Design and analysis of a noncollinear acousto-optic tunable filter," *Opt. Lett.*, vol. 32, no. 16, p. 2417, Aug. 2007.

[27] X. Zhang, C. Zhang, Y. Chen, H. Wang, Z. Sheng, X. Huang, Z. Tan, W. Qiu, P. Wang, R. Zheng, X. Zeng, R. Lai, and J. Yu, "Study on the performance of double filtering based on an acousto-optic tunable filter," *Phys. Scripta*, vol. 94, no. 11, Nov. 2019, Art. no. 115507.

[28] B. Xue, K. Xu, and H. Yamamoto, "Discussion to the equivalent point realized by the two polarized beams in AOTF system," *Opt. Express*, vol. 4, no. 3, p. 139, Feb. 1999.

[29] L. Ding and Y. Li, "Study of imaging resolution for TeO_2 noncollinear AOTF," *Proc. SPIE*, vol. 2918, pp. 102–107, Jan. 1997.

XIAOFA ZHANG received the B.S. degree in measurement technology and instrument from Jiaxing University, China, in 2017. He is currently pursuing the master's degree in optical engineering with Fujian Normal University.

His research interests include the design application of acousto-optic tunable filter and image processing.

CHUNGUANG ZHANG received the Ph.D. degree in physical electronics from the Harbin Institute of Technology, Harbin, China, in 2009.

Since 2009, she has been an Associate Professor with the College of Photonic and Electronic Engineering, Fujian Normal University, Fuzhou, China. Her research interests include hyperspectral microscopic imaging, and the design of acousto-optics filters and hyperspectral imaging systems.

YUPUYUN WANG was born in Tangshan, Hebei, China, in 1999. She is a Sophomore majoring in optoelectronic information science and engineering with Fujian Normal University. She set up a College Student Innovation and Entrepreneurship Project Group with her classmates and served as the Group Leader.

HAO WANG received the Ph.D. degree in physical electronics from the Harbin Institute of Technology, Harbin, China, in 2009.

Since 2009, he has been an Associate Professor with the College of Photonic and Electronic Engineering, Fujian Normal University, Fuzhou, China. His research interests include the design of hyperspectral imaging systems, hyperspectral microscopic imaging, and nonlinear optics.

ZHENFEI SHENG was born in Anshan, China, in 1994. He received the B.S. degree in optoelectronic electronic information science and engineering from the Shenyang University of Technology. He is currently pursuing the M.S. degree in optical engineering with Fujian Normal University.

He currently specializes in the computer vision of deep learning and medical related image processing.

ZHIWEI TAN was born in Yancheng, Jiangsu, China, in 1996. He received the B.S. degree from the Xuzhou Engineering College, China, in 2018. He is currently pursuing the master's degree in optical engineering with Fujian Normal University.

WEIJIE QIU was born in Lianyuan, Hunan, China, in 1997. He received the B.S. degree from Jushou University, China, in 2018. He is currently pursuing the master's degree in optical engineering with Fujian Normal University.

XI HUANG received the B.S. degree in physics and the M.S. degree in photonics from Fujian Normal University, China, in 1994 and 2005, respectively.

Since 2005, he has been an Associate Professor with the College of Photonic and Electronic Engineering Department, Fujian Normal University. His research interests include the parallel processing of artificial neural networks based on FPGA, applications of AI technology, embedded systems, and the IoT.

PENGCHONG WANG received the Ph.D. degree in physical electronics from the Harbin Institute of Technology, Harbin, China, in 2017.

He is currently a Postdoctoral Researcher with the Xi'an Institute of Optical Precision Machinery, Chinese Academy of Sciences, Xi'an, China. His main research interests include acousto-optic modulation and Fourier transform infrared spectrum imaging technology.

WENYAO LIU received the M.S. degree in integrated traditional Chinese and western medicine from the Fujian University of Traditional Chinese Medicine, China, in 2012.

He is currently the Director of the Medical Management Department, the affiliated hospital of Fujian Normal University. His research interests are to specialize in the treatment of chronic gastritis, peptic ulcer, chronic cough, cough variant asthma, urinary tract infection, urinary stones, and other diseases with integrated traditional Chinese and western medicine.

HAIPING TONG was born in Longyan, China, in 2000. He graduated from the No. 1 Middle School, Fujian, China, in 2018. He is currently pursuing the B.S. degree in optoelectronic information science and engineering with Fujian Normal University.

YUHAO LIU was born in Fuzhou, China, in 2000. He received the degree from the Fuzhou No.1 High School, in 2018. He is currently pursuing the B.S. degree in optoelectronic information science and engineering with Fujian Normal University.

He has a strong interest in photoelectric information technology and devotes himself to the field of photoelectric information processing.

XIANSHENG WANG was born Quanzhou, China, in 2000. He is a Sophomore majoring in optoelectronic information science and engineering with Fujian Normal University. He is an Outstanding Member of the Communist Youth League of Fujian Normal University. He has won the first prize of the Huawei ICT Competition.